Ultrafast-Laser Driven Plasma for Space Propulsion

CP01-01 NIAC Phase II Subcontract 0765-003-003

Final Report

Terry Kammash
University of Michigan

Ultrafast-Laser Driven Plasma for Space Propulsion

CP01-01 NIAC Phase II Subcontract 0765-003-003
Final Report

Terry Kammash
University of Michigan, Ann Arbor, MI 48109

Abstract

Much progress has been made in recent years in the area of accelerating charged particles to relativistic speeds by ultrafast lasers. In table top-type experiments at the University of Michigan and other laboratories, charge-neutral proton beams containing more than 10^{14} particles with mean energies of tens of MeV have been produced when high intensity lasers with femtosecond pulse lengths are made to strike thin solid targets. When viewed from a propulsion standpoint such systems can produce specific impulses of more than one million seconds albeit at modest thrusts making them especially suitable for interstellar missions. Several schemes have, however, been proposed to enhance the thrust so as to make these systems suitable for manned interplanetary missions. In this report we summarize the underlying physics principles that make relativistic plasmas driven by ultrafast lasers particularly attractive for propulsion applications. We introduce the "Laser Accelerated Plasma Propulsion System" LAPPS, and demonstrate its potential propulsive capability by addressing an interstellar mission to the Oort cloud, and another within the solar system. Using these examples we identify the major technological problems that must be addressed if this system is to evolve into a leading contender among the advanced propulsion concepts currently under investigations. We conclude that thrust enhancement is critical and suggest two approaches to address it. One involves accelerating heavier (than proton) ions such as carbon or fluorine, or even lead in some instances, and another involving irradiating larger focal spots. The latter

provides enhancement through larger population of emitted particles as well as measurable increase in their velocity which in turn contributes to an increase in thrust. The other important issue has to do with rep rates especially on the target side to match that on the laser side. We find that large rep rates leading to nearly steady state operation can be achieved by utilizing jet targets, and our research reveals that carefully chosen fluids can indeed serve as suitable targets in a propulsion system with no discernable obstacles to overcome.

Nomenclature

a_o = modified vector potential
A = vector potential, area
B = magnetic field
c = speed of light
c_s = ion sound speed
d = electron cloud diameter, hydraulic diameter
D = linear distance, jet diameter
e = electron charge
E = electric field
E_z = accelerating electric field
E_e = electron energy
E_i = ion energy
F = thrust
g = earth's gravitational acceleration
h = electron cloud thickness
I = laser intensity
I_{sp} = specific impulse
k_o = laser wave number
m_i = ion mass
M_i = initial vehicle mass
M_f = final vehicle mass
n = index of refraction
n_b = electron beam density
N_i = ion beam population
p = particle momentum
r_e = classical electron radius
R = electron cloud radius
S_f = distance to destination
t_i = ion acceleration time
t_f = time to destination
T_e = electron temperature
v = particle velocity, fluid velocity
v_e = exhaust velocity
V_f = final vehicle velocity
v_i = ion velocity
Z = ion charge
γ = relativistic parameter
λ = laser wave length
ω_o = laser frequency
ω_p = plasma frequency
Re = Reynolds number
η = kinematic viscosity
P = perimeter
L = length
t = thickness
L_d = distance for droplet formation
ρ = fluid density
σ = surface tension

II. Introduction and Basic Principles

One of the remarkable scientific developments in laser technology in recent decades is the steady increase in their peak power and focus ability[(1)]. Advanced laser systems now have multi megawatt peak powers (See Fig 1) and, when focused on micron spot sizes, can produce electromagnetic intensities approaching $I=10^{21}$ w/cm^2. The associated laser electric fields exceed

10^{11} V/cm and can readily accelerate electrons to their rest mass energies if applied over a distance of several microns as noted in Fig 1. In fact it is suggested that peak powers may soon be reached that will accelerate protons to their rest mass energy of 938 MeV. This means that these particles, when ejected from a propulsion device, will travel at 0.866 the speed of light, and that translates to specific impulses of well over 10 million seconds. The implication of theses facts for space propulsion are truly staggering especially, when coupled to the fact that rep rates of kilohertz have also been achieved for high intensity lasers.

Although no exact theory for the acceleration mechanism currently exists, it is possible to produce a plausible, heuristic analysis consistent with sound physics principles that will generate mathematical expressions that can predict experimental results with some measure of accuracy, consistency and reliability. These expressions can also be employed to predict the propulsive capability of these systems when they eventually evolve into viable propulsion devices.

Since the laser-electron interaction lies at the heart of the ion acceleration process, we begin by examining the dynamics of an electron in the fields of the high-intensity laser. The starting point is the relativistic Lorentz equation given by[2]

$$\frac{d}{dt}\left(\underset{>}{p}\right) = \frac{d}{dt}\left(\gamma m_o \underset{-}{v}\right) =$$

$$-e\left[\underset{>}{E} + \frac{\underset{>}{v} \times \underset{-}{B}}{c}\right] \qquad (1)$$

where

$$\gamma = \left(1 - v^2/c^2\right)^{-1/2} \qquad (2)$$

is the familiar relativistic parameter, m_o the rest mass of the electron, c the speed

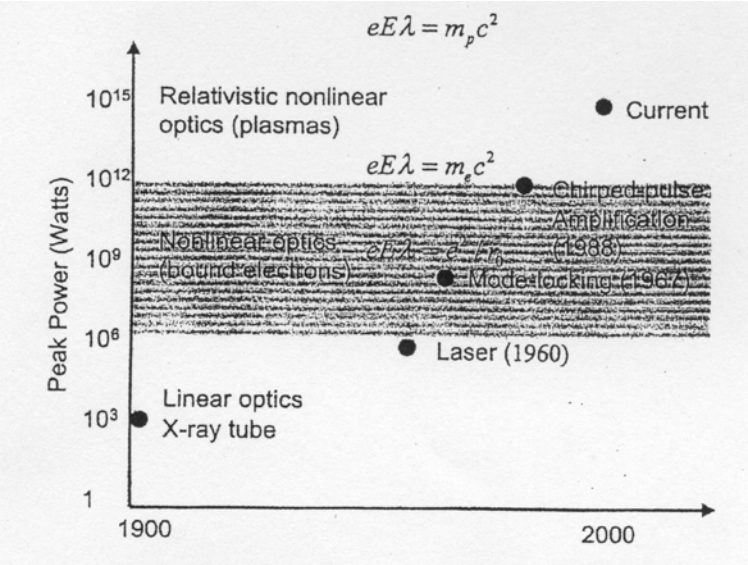

Fig 1. Peak Power History

of light, e the electron charge, v its velocity, and E and B the electric and magnetic fields of the incident radiation respectively. For a linearly polarized electromagnetic wave propagating in the z-direction, and the axis of laser polarization along the x-direction the fields can be expressed by

$$\underset{>}{E} = \hat{x}\, E_o \sin\left(k_o z - \omega_o t\right) \qquad (3)$$

$$\underset{-}{B} = \hat{y}\, B_o \sin\left(k_o z - \omega_o t\right) \qquad (4)$$

where $\hat{x}, \hat{y}$ are unit vectors in these directions, k_o the wave number and ωo the frequency of the wave. Upon substitution of (3) and (4) into (1) and expressing the fields in terms of the vector potential *A* a solution can be found[3] that reveals that the electron will "quiver" and execute a figure of eight trajectory as shown in Fig 2, and an average drift motion along the direction of laser propagation. The spatial extent of the "quiver" is determined by the modified vector potential a_o given by

$$a_o = \frac{eA}{m_o c^2} = 0.85 \times 10^{-9} \sqrt{I\left(w/cm^2\right)}\ \ \lambda(\mu m) \qquad (5)$$

where λ is the laser wave length. It should be noted that a_o is related to the relativistic parameter γ through

$$\gamma = \left[1 - v^2/c^2\right]^{-1/2} = \left(1 + \frac{a_0^2}{2}\right)^{1/2} \qquad (6)$$

hence the connection between the laser parameters and the velocity (or acceleration) of the electron with which it interacts. The electron motion depicted in Fig 2 has been confirmed experimentally[4] in the first major effort to study relativistic non-linear optics especially as it applies to the non-linear "Thomson Scattering" phenomenon noted in Fig 1.

When a high-intensity laser strikes a target, it produces at the surface a plasma (often referred to as the "blow-off" plasma) with a size of about half a

laser wavelength[5] due to the longitudinal electron oscillations resulting from the oscillating Lorentz force. Twice in a laser period the electrons of this plasma re-enter the target while the ions remain virtually immobile due to their large mass. Returning electrons are accelerated by the "vacuum" electric field and subsequently deposit their energy inside the target. The electrons of the plasma become strongly heated by the laser light, penetrate deeper inside the solid target with relativistic speeds, and form a relatively low-density, high-energy component of the entire electron population.

These high-energy electrons create an electrostatic field which accelerates ions in the forward direction while decelerating the electrons until both species drift out at same rate. An electrostatic field near the target surface has a bipolar structure with the more pronounced component accelerating ions in the forward direction. If the laser pulse duration is longer than the ion acceleration time in the layer then the ions would acquire an energy equal to the electrostatic energy. Since this "ambipolar" potential causes both the electrons and ions to proceed at the same rate, they emerge from the back surface of the target in a perpendicular direction in a "neutral" nearly collimated beam form as shown in Fig 3. This emerging beam of charged particles is what provides the thrust in a propulsion device.

It is instructive at this point to present a mathematical formulation of the acceleration mechanism just described, and for that we will employ the electron cloud motel[6] illustrated in Fig 4. In this one-dimensional model we assume that the energetic electrons,

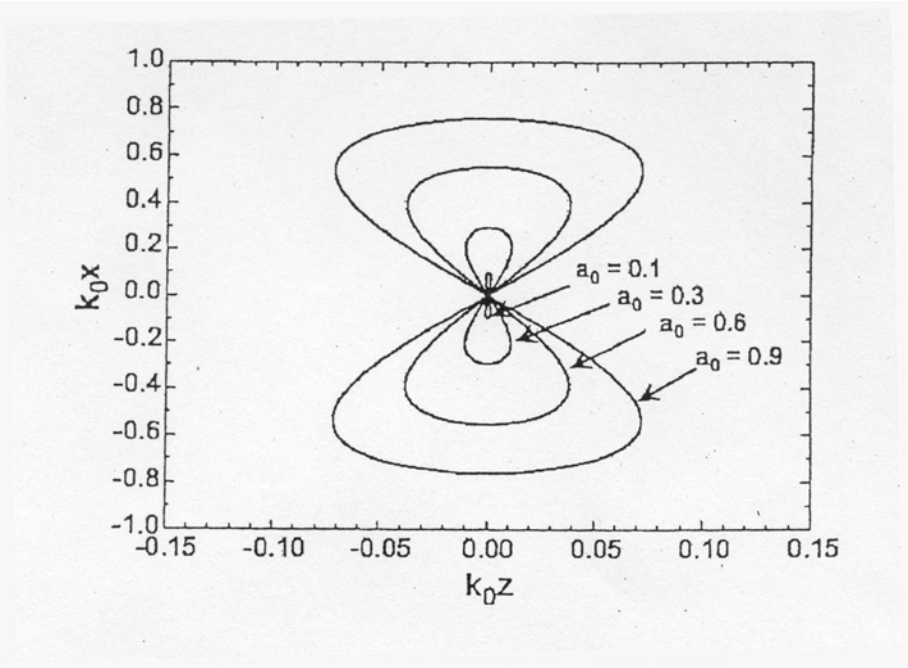

Fig. 2. Trajectory of an electron in a linearly polarized laser field as a function of laser intensity

alluded to earlier, form a relativistic electron beam of density n_b in the form of a disc-like (pancake) cloud of radius "R" and thickness "h". To calculate the accelerating electric field, E_z, we begin with the Poisson equation, namely

$$\nabla . \underset{>}{E} = -4\Pi e n_b \qquad (7)$$

which can be readily shown to yield

$$E_z \approx 2\Pi e\, n_b\, h \qquad (8)$$

where we have neglected the radial component of the electric field due to the assumed smallness of h/d ratio. Implicit in the above result is the fact that the electrostatic field E_z is created by the surface charge en_bh. If we further invoke the energy conservation for the electrons in the cloud, then we can write

$$\left(\gamma_b - 1\right) m_o c^2 = \Pi e^2 n_b h^2 \qquad (9)$$

from which we can solve for the thickness of electron cloud "h" to be

$$h = \sqrt{\frac{\gamma_b - 1}{\Pi n_b r_e}} \qquad (10)$$

where

$$r_e = \frac{e^2}{m_o c^2} \qquad (11)$$

is the familiar classical electron radius. Upon substitution of (10) into (8) we find

$$E_z \approx 2c\sqrt{\Pi m_o \left(\gamma_b - 1\right) n_b} \qquad (12)$$

For a beam density of 10^{19} cm^{-3} and γ_b=10 the thickness of the charge separation layer is about 10μm and the corresponding electric field is about 900 GV/m. The energy gained by an electron accelerated by such a field is eE_zh, and this corresponds to about 9 MeV. Since ions are also accelerated by the same electric potential then the ion energy, which is equal to ZeE_zh is also about 9 MeV in the case of a proton whose Z=1. While the above formulation is particularly useful in explaining the underlying principle of ion acceleration by ultrahigh intensity lasers it falls short in terms of its utility

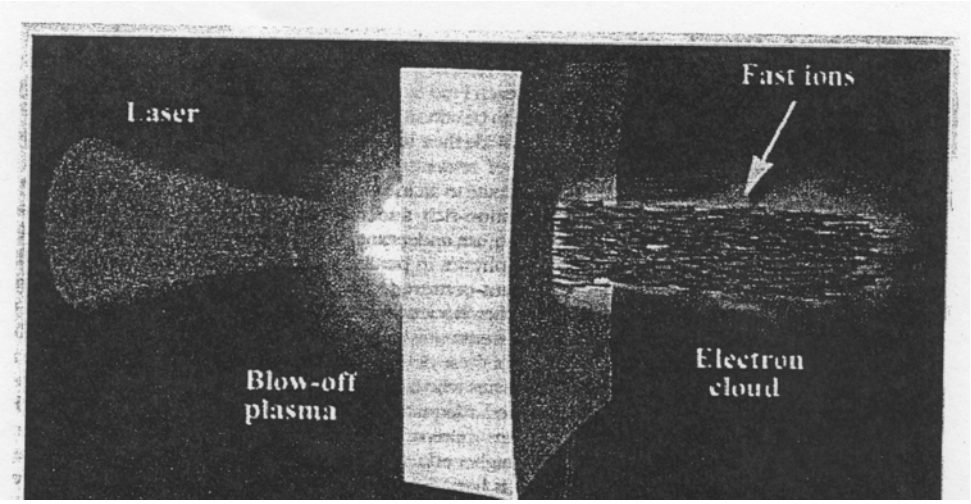

Fig. 3. Ultrafast Laser Impinging Upon a Target to Produce Fast Ions.

for space propulsion applications since it does not connect the energy of the ejected particles to the parameters that characterize the laser beam and the target it strikes. To address this vital relationship we invoke another energy (power) balance; this time between the incident laser beam and the electrons in the cloud, namely

$$\left(n_b(\gamma_b - 1)m_o c^2\right)c = \eta I \qquad (13)$$

where η represents the efficiency of the energy transfer i.e. the efficiency of laser-energy conversion into high-energy electrons. Denoting this energy be E_e we find from the above equation

$$E_e = \frac{\eta I}{n_b c} \qquad (14)$$

Moreover, we note that an electron must have an energy that exceeds the Coulomb energy in order to penetrate deeper into the target and ultimately produce the electrostatic potential, hence

$$E_e \approx \Pi e^2 n_b h R \qquad (15)$$

where R is the radius of the focal spot. Solving for n_b from EQ (15) and substituting into (14) we get

$$E_e \approx \sqrt{\frac{\Pi e^2}{c} I \eta R h} \qquad (16)$$

and noting further that in most cases of interest $h \approx \lambda$ we can also write

$$E_e \approx \sqrt{\frac{\Pi e^2}{c} I \eta R \lambda} \qquad (17)$$

If we now express the laser intensity in units of 10^{18} w/cm^2, and the spatial scales in microns, then the above expression gives the electron energy in MeV and, correspondingly, the ion energy i.e.

$$E_i = Z E_e = Z\sqrt{I \eta R \lambda} \ \text{MeV} \qquad (18)$$

Although, as noted earlier, the above formulation is heuristic and based on sound physics principles, its usefulness in propulsion applications is vindicated by some fairly current experimental validation. For example, in a recent experiment[7] a 10 TW hybrid Ti:

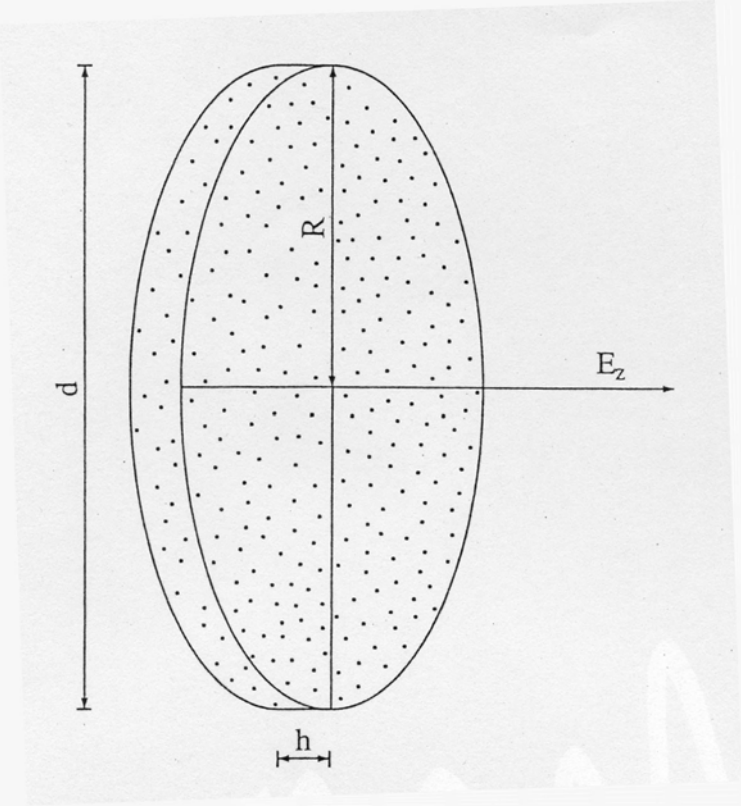

Fig. 4. Electron Cloud Model

sapphire/Nd: phosphate glass laser, which was able to deliver up to 4 J in 400 fs pulse at different wave lengths, was focused on the surface of thin films of Aluminum and Mylar with variable thicknesses to produce protons of several MeV energy.

The results are depicted in Fig 5 where we note that a wave length of 1.053 μm was used in the Mylar target, and a 0.532 μm wavelength in the case of Aluminum. We readily observe that the ratio of maximum proton energy of Mylar to Aluminum, namely 3.2/2.3, is almost exactly that of the square root of the corresponding wavelengths. Furthermore, we note that the maximum proton energy appears to occur at target thickness of about 10μm independent of the material of the target. This seems to indicate that maximum ion energies can be achieved when the target thickness is about 10 wavelengths. Additional validation of Eq (18) can be obtained by focusing on one of the experimental points reported in the above-mentioned experiment. In that instance, a laser intensity of 3×10^{18} w/cm^2 was employed on a focal spot of radius R=5 μm In an Aluminum target with thickness of 1.4 μm in which the electron density in the ablated plasma that gives rise to the charge separation, was estimated to be 10^{20} cm^{-3}. Using Eq (8) we find that the accelerating electric field $E_z \approx 900$GV and over a distance of 1.4 μm the electron gains an energy of about 1 MeV, and correspondingly the proton acquires the same energy. This is reasonably well verified in Fig 5. In this experiment the energy transfer efficiency of was estimated at $10^{0/0}$ and if we insert this value along with the other parameters in Eq (18) we find once again that the proton energy is about 1 MeV. The dependence of the ion energy

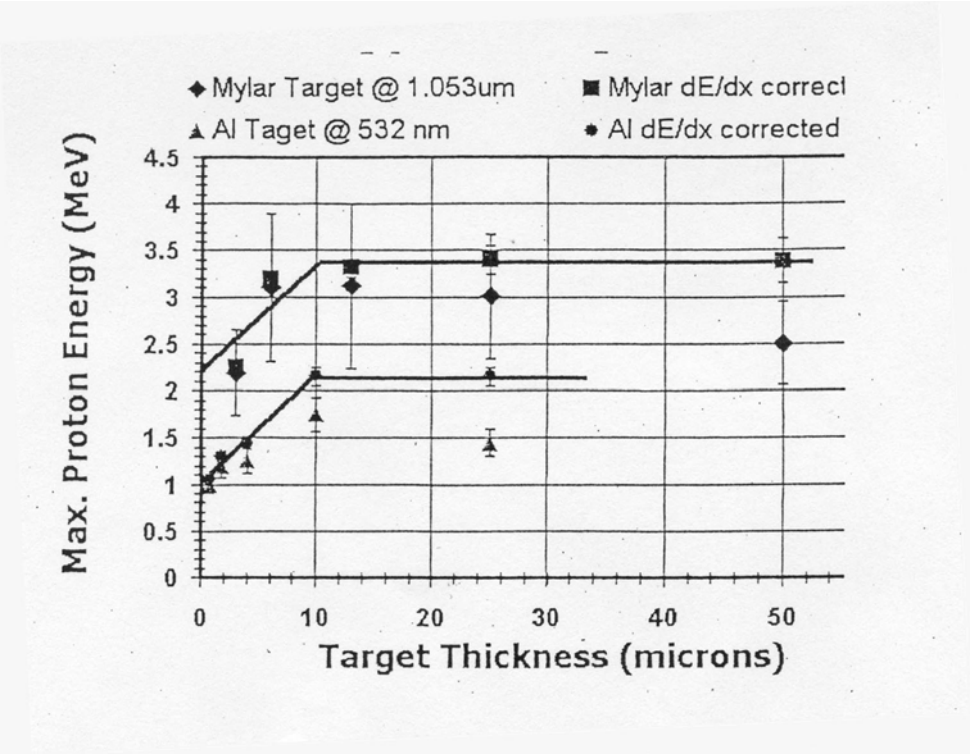

Fig. 5. Maximum Proton Energy Versus Target

on the square root of the intensity as displayed by Eq (18) has been verified experimentally at many laboratories as shown in Fig (6). It is interesting to note that for laser intensities lower than 10^{19} w/cm^2 the variation is nearly linear while for intensities higher than this value the variation is indeed with $\sqrt{I}$ and that is the regime of interest to propulsion applications as we shall see shortly.

Before concluding this section it would be useful to point out that the plasma ablated when a high intensity laser strikes a target, plays another critical role in the process of charged particle acceleration to relativistic energies. This manifests itself through the collective effects where, for example, at these high intensities the relativistic change in the electron mass alters the plasma frequency:

$$\omega_p = \omega_{po} \Big/ \gamma^{1/2} = \left(4\Pi n_e e^2 / \gamma m_o\right)^{1/2} \qquad (19)$$

where

$$\omega_{po} = 5.64 \times 10^4 \, n_e^{1/2} \text{ rad/s} \qquad (20)$$

is the plasma frequency in a quiescent plasma, n_e the plasma electron density and $\gamma = \sqrt{1 + a_0^2}$ the relativistic Lorentz factor introduced in Eq (6). This in turn alters the dielectric properties of the plasma medium through the modification of the index of refraction of the light wave given by

$$n = \left[1 - \left(\omega_p / \omega_o\right)^2\right]^{1/2} \qquad (21)$$

where ω_o is the light frequency. If there is an on-axis maximum of the radial profile of γ, such as created by a laser beam with an intensity profile peaked on axis, then the index of refraction n(r) can have a maximum on axis. By causing the wave front to curve inward and the laser beam to converge, this will result in optical guiding of the laser light. Since the laser phase velocity, v_p, depends on

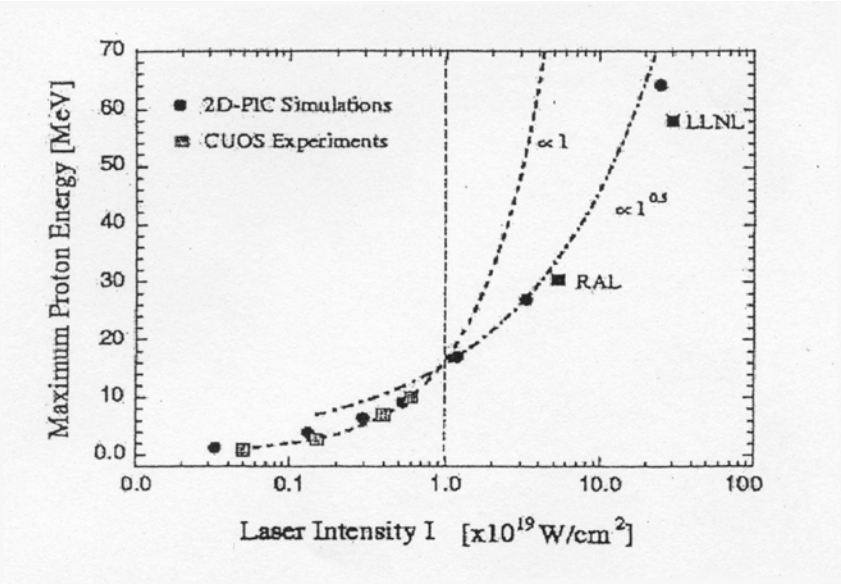

Fig. 6. Scaling of Maximum Proton Energy with Laser Intensity $\lambda = 1$ μm

the index of refraction, $v_p = c/n$, it will then depend on the laser intensity. Local variation in the phase velocity will modify the shape of the laser pulse, and consequently, the spatial and temporal profile of the laser intensity. This so-called "relativistic self-focusing" occurs when the laser power exceeds a critical power given by

$$P_c = 17\left(\frac{\omega_o}{\omega_p}\right)^2 GW \qquad (22)$$

For the experimental parameters noted earlier, namely $n_e = 10^{20}$ cm^{-3}, an electron energy of about 1 MeV, a relativistic parameter $\gamma = 2.76$ and for a laser wavelength of about 1 μm, the corresponding laser frequency ω_o is about 19 x10^{14} rad/sec, while $\omega p \approx 1.1$ x10^{14} as obtained from EQ (19). Putting these values in EQ (22) we find that the critical power, Pc, is about 5 TW which is significantly less than the 10TW utilized in the experiment, indicating that relativistic focusing was indeed in affect in that study. It is also worth noting that not only can the plasma affect the light but the light can affect the plasma. The electrons are pushed to regions of lower light intensity by the "ponderomotive" force which is proportional to the gradient of the light pressure. A Gaussian-shaped laser intensity profile will tend to expel electrons radially from the axis often referred to as "electron cavitations". Eventually, the charge displacement due to expelled electrons will move the ions, forming a channel with a density depression on axis, i.e. $n_e(0) < n_e(r)$. Again $\gamma(o) > \gamma(r)$ results, enhancing relativistic self-guiding or allowing a second trailing laser pulse to be guided. Such density channels have also been created by thermal gradients, which are produced by long-duration

laser pulses, and the focusing phenomenon just described is often referred to as "ponderomotive self-channeling". It is abundantly clear that these focusing effects are important from the standpoint of propulsion application since they ultimately contribute to the efficient transfer of energy from the laser beam to the ejected charged particles by sustaining the focusability on target.

While the result of Eq (18) regarding the ion energy produced by laser acceleration appear satisfying from the point of view of propulsion, it does not take into account the effects of the plasma expansion in vacuum driven by the hot electrons. Two asymptotic regimes of ion acceleration are known to arise: the regime of isothermal expansion[8] where the electron temperature remains constant, and the regime of adiabatic expansion[9,10] where the total energy of the expanding plasma is conserved. It is reasonable to assume that the isothermal regime is relevant for long laser pulses, namely for $\tau > t_i$ where t_i is the ion acceleration time given by

$$t_i = \frac{h}{v_i} \qquad (23)$$

For the experiment of Ref 7, we recall that h = 1.4 μm and an ion energy of about 1 MeV gives a velocity $v_i \approx 1.33 \times 10^7$ m/s. This leads to $t_i \approx 10^{-13}$ seconds which is significantly shorter than the laser pulse length, τ of 400 femtoseconds. This isothermal expansion leads to the following expression for the maximum ion velocity[11]:

$$v_{imax} = 2C_s \ln(d/h) \qquad (24)$$

where

$$C_s = \sqrt{\frac{ZTe}{m_i}} \qquad (25)$$

is the ion sound speed, and "d" and "h" are the diameter and thickness of the focal spot as presented earlier. In Eq (25) T_e denotes the electron temperature

and m_i the ion mass. For the case at hand $C_s \approx 3.9 \times 10^7$ m/s and for $d/h \approx 5$, $v_{imax} = 3.9 \times 10^7$ m/s and that represents a three fold enhancement in the ion velocity, and correspondingly in the specific impulse. In the adiabatic regime, the ion distribution is steeper and assumes a Maxwellian form for which the maximum velocity is given by[6]

$$\mathbf{V}_{imax} = 2\sqrt{2}\, C_s \ln(d/h) \qquad (26)$$

The above results reveal in a dramatic fashion that the energy of the accelerated ions ultimately depends on the electron energy (through T_e), and the duration of the pulse. It is further suggested that ion acceleration would be more efficient with increasing focal spot size, a fact that will not go unnoticed when thrust enhancement of this system is considered.

The LAPPS Propulsion System

An artist's conception of a propulsion vehicle based upon the analysis presented above is displayed in Fig. 7. The "Laser accelerated plasma propulsion system" LAPPS shown, makes use of a high-intensity laser, which derives its electric power from a nuclear reactor via a power conversion scheme. The energized laser strikes a target whose rep rate is matched to that of the laser to produce thrust by way of the ejected energetic charged-particle beam. To assess the propulsive capability of such a system we assume that its relevant parameters are comparable to those produced in recent experiments[12, 13]. In these experiments, an intense collimated beam of high-energy protons was emitted from the rear surface of thin solid targets irradiated at one petawatt (10^{15}) power, and peak intensity of 3×10^{20} w/cm^2. A

maximum proton energy of 58 MeV was observed, and approximately half of the kilojoule laser energy (i.e. 500J) was believed to appear in the particle beam. The focal spot size was 9 μm and the thickness of the gold foil irradiated was 125 μm. If we now employ Eq (18) for the laser and target parameters just cited, we find that the energy of the ejected protons is 5.3 MeV which is about the same as the mean energy observed i.e. 6 MeV. An energy balance for the particles in the beam reveals that it contained 6×10^{14} particles, and if a rep rate of 1 kHz is assumed then such a beam is capable of producing about 30 milli-Newtons. It should be noted that in the above-mentioned experiments the amount of laser energy that appeared in the ejected proton beam was distributed among protons of different energies. For example, 12% of the laser energy was transferred to 2×10^{13} protons of energy >10 MeV while the spectrum exhibits a high-energy cutoff as high as 58 MeV. For the purposes of this calculation, it was assumed that the 500 J were transferred to 6×10^{14} protons at a mean energy of 5.3 MeV. In the case of heavier ions such as carbon and fluorine (to be addressed shortly) Ref 19 notes that by using high-intensity laser pulses (such as those contemplated for LAPPS) an efficiency of well over 5% was achieved in ion acceleration to more than 5 MeV/nucleon from the rear surface of thin-foil targets. It should also be noted that while a 1 kJ laser operating at 1 kHz generates a thrust of about 3 mN, and thus one might entertain the thought of simply using the laser beam to provide momentum, the fact remains that in LAPPS it is not the laser (photon) momentum that matters, rather it is the laser power (and correspondingly the intensity) that counts since the

accelerating electric field scales with laser intensity as shown in Eqs (5) and (6). In other words, larger particle energies can be achieved through manipulation of pulse length without changing the energy or the rep rate of the laser. These facts are summarized in Table 1.

Table 1
Present Day LAPPS Parameters

1. Proton Beam
   - i) particle population = 6×10^{14}
   - ii) mean energy = 5.3 MeV
   - iii) maximum energy = 58 MeV
   - iv) Beam energy = 500 J
2. Laser Beam
   - i) wavelength = 1μm
   - ii) pulse length = 500 fs
   - iii) Intensity = 3×10^{20} W/cm^2
   - iv) Energy = 1 kJ
3. Target
   - i) material = Gold Foil
   - ii) thickness = 125 μm
   - iii) focal spot size = 9 μm
4. LAPPS Propulsion Parameters
   - i) Rep Rate = 1 kHz
   - ii) Specific impulse = 3.2×10^6 s
   - iii) Thrust = 30×10^{-3} N
   - iv) Nuclear System = 1 MWe
   - v) Vehicle Dry Mass = 1-5 mT

The vehicle dry mass was assumed to be primarily that of the nuclear reactor and the power conversion components. These values are based on a recent design[14] (see Table 2) of a multimegawatt nuclear power system that employed a Brayton cycle for its power conversion, and yielded the following results for the mass to power ratio: i) Near term: 5 mT/MWe, ii) Mid term: 2MT/MWe, iii) Far Term: 1 mT/MWe. The range in the vehicle dry mass indicated in table 1 is a reflection of these values, which will be utilized in the mission examples addressed below.

IV Examples of LAPPS Missions

The effectiveness of a LAPPS propulsion system based on current experimental data is addressed by examining two missions: a robotic fly-by, interstellar mission to the Oort cloud, and a round trip journey to Mars. The first case can be viewed as a precursor

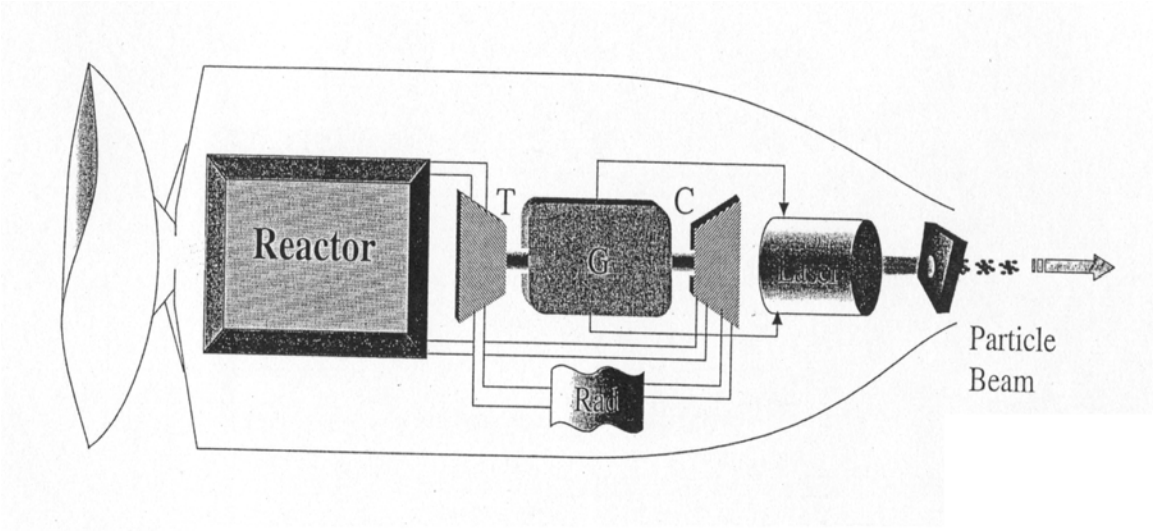

Fig. 7. Laser-Accelerated Plasma Propulsion System (LAPPS)

Table 2.

Design of 160 MW Nuclear Power System (Brayton)
(Lee Mason, NASA GRC) Ref 14
Masses in kg

System Sizing	Near Term	Mid Term	Far Term
Reactor/Shielding	121978	102140	79593
(1) Reactor	115307	96163	74399
(1) Inst. Shield	4923	4386	3694
(0) Crew Shield	0	0	0
(1) PHTs	1748	1591	1500
Power Conversion	17433	15513	14749
(10) TAC/Ducts	182	182	181
(10) Recuperators	916	805	775
(10) Coolers	487	424	384
(10) Structures	158	141	134
Heat Rejection	110756	42080	8810
(1) Radiator	110756	42080	8810
(1) Aux. Equip	0	0	0
Power MGMT & Dist.	534155	161079	77157
(1) Electronics	234756	92061	34709
(1) Radiator	83137	28696	25592
(1) PL Rad.	57905	28953	14476
(1) Cabling	158357	11370	2379
Total	784322	320813	180309
Ratio	4.9 kg/kW = 4.9 mT/MW	2.0 kg/kW = 2.0 mT/MW	1.1 kg/kW = 1.1 mT/MW

mission to the nearest star – Alpha Centauri – which is often cited as the ultimate challenge to accomplish in a scientist's life time. The second is examined because of the current interest of landing humans on the red planet in the not too distant future. For the first mission the equations of interest are[15]:

$$t_f = \frac{M_i - M_f}{F} v_e \qquad (27)$$

$$S_f = \frac{M_i v_e^2}{F} \left[1 - \frac{M_f}{M_i} + \frac{M_f}{M_i} \ln\left(\frac{M_f}{M_i} \right) \right] \qquad (28)$$

$$v_f = v_e \ln\left[\frac{1}{1-\frac{F t_f}{M_i v_e}}\right] \qquad (29)$$

where t_f is the one-way travel time to destination, M_i the initial mass of the vehicle, M_f the dry mass, v_e the exhaust velocity, S_f the one-way distance to destination and V_f the final vehicle velocity at destination assuming it started from rest. For the second mission, we employ a constant thrust, acceleration/deceleration type of trajectory which yields for the round trip time τ_{RT} between two points separated by the linear distance, D, the expression[16]

$$\tau_{RT} = \frac{4D}{g I_{sp}} + 4\sqrt{\frac{D M_f}{F}} \qquad (30)$$

where g is the earth's gravitational acceleration, Isp the specific impulse and F the thrust. Note, in the above equation, that the contributions of the thrust and specific impulse terms are additive and must therefore be somewhat comparable in order to produced a reasonably optimum travel time. It is clear that a system that produces an extremely large Isp at a very modest F will not satisfy such a condition, and will result in a very long trip time.

In the case of the Oort cloud, S_f = 10,000 astronomical units, and for a LAPPS that accelerates protons, the travel time as a function of thrust is shown in Fig 8. The results are given for two values of the final (dry) mass of the vehicle, a far-term value of 1 mT and a near-term value of 5 mT. It is seen that in the latter case the travel time is about 698 years at the present-day thrust of about 30×10^{-3} Newtons, while for the 1 mT case, at the same thrust, the trip time is about 313 years. We further observe that the travel time drops to 26 years for the 5 mT case, and to 12 years for the 1 mT case upon increasing the thrust to 25

Newtons. These travel times become progressively shorter at larger and larger thrusts indicating that such interstellar missions can indeed be accomplished in a human's lifetime. It should be pointed out that the 5 mT case may be viewed as not-too-near term if a laser's electric efficiency of about 20% is taken into account when computing the electric power requirements of the laser. It has been suggested however, that a 40% efficiency for high intensity lasers is indeed within reach making the above travel time estimates realistic and perhaps achievable in the not too distant future.

The linear distance "D" from Earth to Mars of 0.52 AU (7.8×10^{10} m) is the shortest between these two planets, and occurs every 26 months when they are both aligned with the Sun. Substituting in Eq (30) and using the propulsive parameters and masses given in table 1 we obtain the results displayed in Fig. 9. Once again we observe the same trend in that, the travel time drops precipitously as the thrust in increased. For the present-day thrust of 30×10^{-3} Newtons, the round trip to Mars is about 5200 days for a vehicle mass of 5 mT, and about 2322 days for the one mT case. As the thrust is increased to 25 Newtons the trip time in the first case drops to 186 days, and to a mere 82 days in the second case, and these times become very short as thrust values are increased to 500 N and beyond. Since LAPPS will be nuclear driven it is interesting to compare it with a nuclear electric propulsion system such as the one given in Ref 17 where missions to Pluto-Charon (among others) were considered. The parameter of interest is "α", which is the mass to jet power ratio, where it is shown that even for modest payloads, a one-way travel time of about 12 years would be the

result if α has a predicted value of 100. A smaller α results in a shorter travel time and an $\alpha = 10$ for LAPPS can result in a much shorter travel time even for the Oort cloud, which is 3-4 orders of magnitude farther than Pluto. Advancements in laser technology should provide enhancements in jet power (through larger velocities and Isp's) without major additions to the mass through significant reductions in pulse lengths. The projected Isp's cannot be matched by any electric propulsion system. The question immediately arises as to what methods can be used to enhance the thrust in a LAPPS propulsion system. The answer may be found in the following expression for thrust:

$$F = N_i m_i \omega v_i \qquad (31)$$

where Ni is the number of ions in the laser-accelerated beam, m_i the ion mass, v_i the ion mean velocity and ω the rep rate. For a fixed ω the remaining parameters in Eq (31) lend themselves to increases that lead to increased in F. The ion population N_i can be increased if larger focal spots are irradiated since the number of these particles increases with the area if the target thickness is kept constant especially near the optimum value alluded to earlier. It is clear that irradiating larger spots require higher power lasers in order to maintain the same intensity, but as noted earlier, it is desirable in many instances to increase the thrust even if it is done as the expense of reducing the velocity (energy) and correspondingly the specific impulse. We recall, however, from Eq (24) that as a result of the plasma expansion in vacuum, some of the thermal energy is converted to kinetic energy and the maximum ion velocity is attained with larger focal diameters. Hence, an increase in the

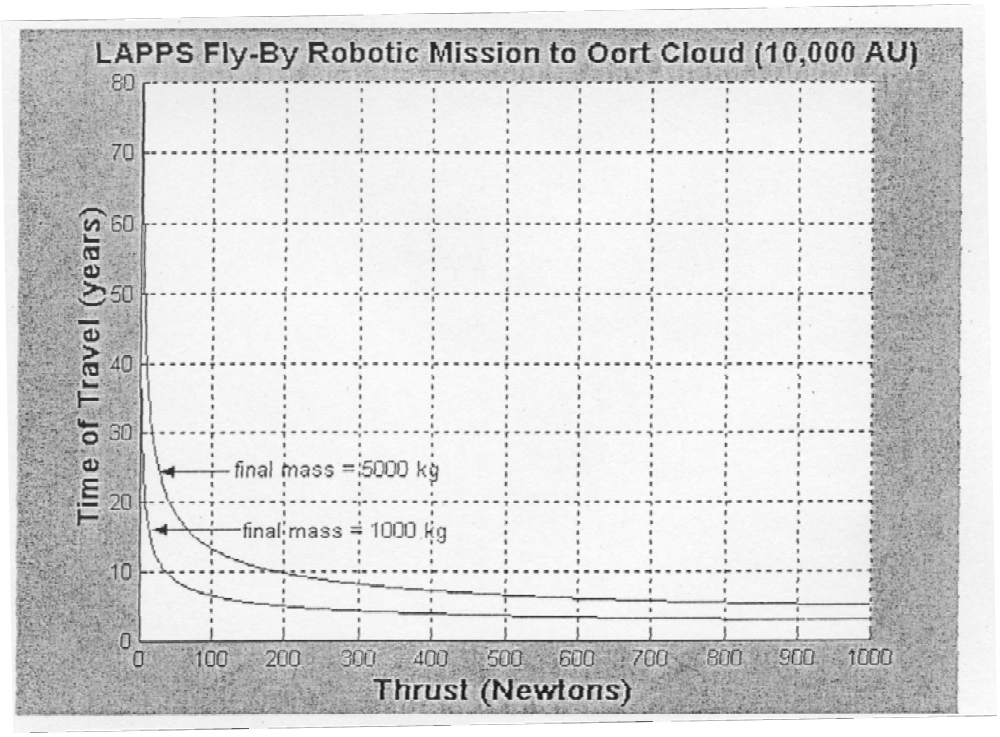

Fig. 8. Oort Cloud Mission with proton beam

irradiated area leads not only to a larger Ni but, interestingly enough, to a larger v_i, thus providing a two-component effect on the thrust.

The third parameter that impacts F is the mass of the ejected ion. In all the analyses presented above, the focus was on protons since they have constituted the major component of the accelerated beams in most of the experimental investigations of this phenomenon. Recently, however, several experiments have succeeded in accelerating heavier ions with the use of ultra higher intensity lasers. For example lead (Pb^{+46}) ions of up to 430 ± 40 MeV energy have been produced form laser-solid interactions at focused intensities of 5 x 10^{19} w/cm$^{2(18)}$, and collimated jets of carbon and fluorine ions of up to 5 MeV per nucleon (~100 MeV) were also observed from the rear surface of thin foil irradiated with laser intensities of up to 5 x 10^{19} w/cm$^{2(19)}$. In the latter case, the normally dominant proton acceleration was suppressed by removing the hydrocarbon contaminants by resistive heating. These experiments were performed with a 100-TW laser for which the pulses (~30J, ~300 fs, 1.05 μm) were focused at normal incidence on a target to an intensity of up to 5 x 10^{19} w/cm^2. A laser-to-ion energy conversion (η) of 0.5% was indicated, and the spectrum of the ejected particles appears to show that the mean ion energy for both species was about 6 MeV which is comparable to the LAPPS values given in table 1. If we normalize the properties of the carbon and fluorine beams to those of the protons, and unitize these values in the two mission examples addressed earlier we obtain the results shown in Figures 10 and 11. In Fig 10, dealing with the Oort cloud mission, we observe the values listed in

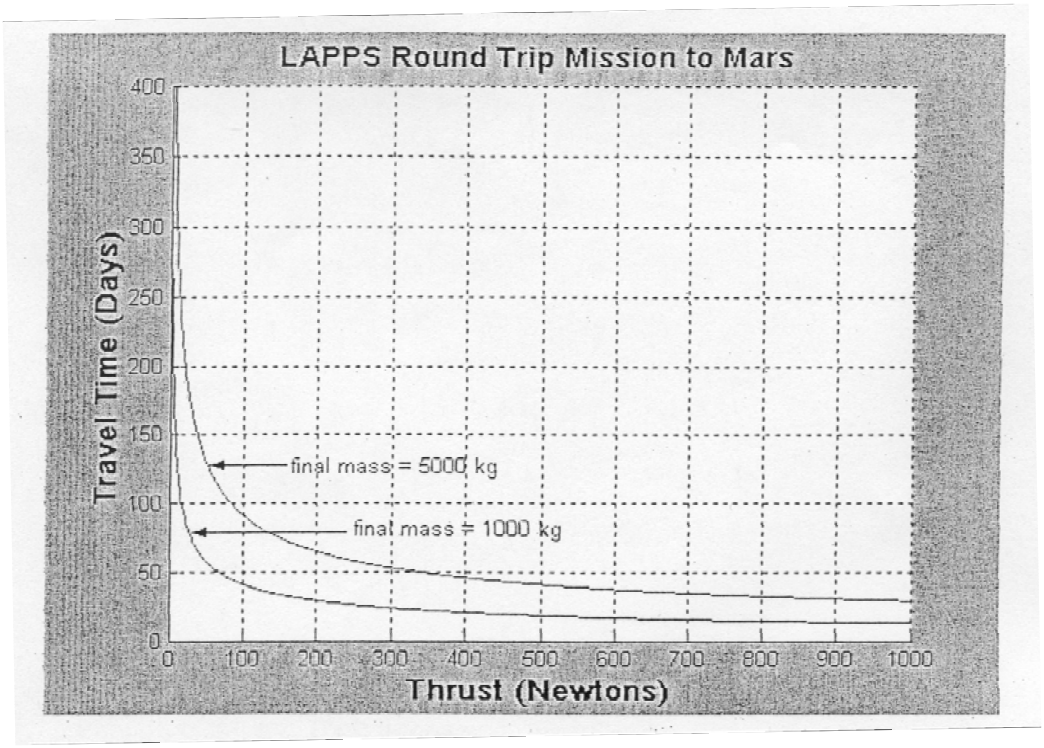

Fig. 9. Mars Mission with proton beam

Table 3. For the Mars mission the results are given in Table 4 and shown in Fig 11. In both instances the velocities – and correspondingly the specific impulses – of the heavier ions were reduced relative to the protons of the same energy but the larger masses more than compensated for that as reflected in the increase in the thrust and correspondingly in the travel time. In short, the successful acceleration of heavy ions by the high intensity lasers, as demonstrated in several recent experiments, provide the basis for future LAPPS propulsion devices that can generate high thrusts and large specific impulses simultaneously.

Liquid Jet Targets

The LAPPS propulsion concept described above assumes 1 kHz rep rate in order to produce the propulsive capability noted. It is somewhat difficult to use solid targets that can be inserted at this rate, and an alternative jet target has been suggested to accommodate this concern. Cryogenic liquid jet targets using nitrogen were employed in experiments in which soft x-ray generation was produced by high energy ultrafast lasers[20]. In order to provide a good target for utilization in LAPPS, the surface of the liquid jet must be smooth necessitating a laminar jet. This is dictated by the Reynolds number given by

$$\mathrm{Re} = \frac{d\, v}{\eta} \qquad (32)$$

where v is the fluid velocity, η the kinematic viscosity, and d the "equivalent" hydraulic diameter, generally defined as the ratio of the channel area to its perimeter. If we assume that the jet is "square" in shape with length L and thickness t, then we can write

$$d = \frac{4A}{P} = \frac{4Lt}{2(L+t)} \qquad (33)$$

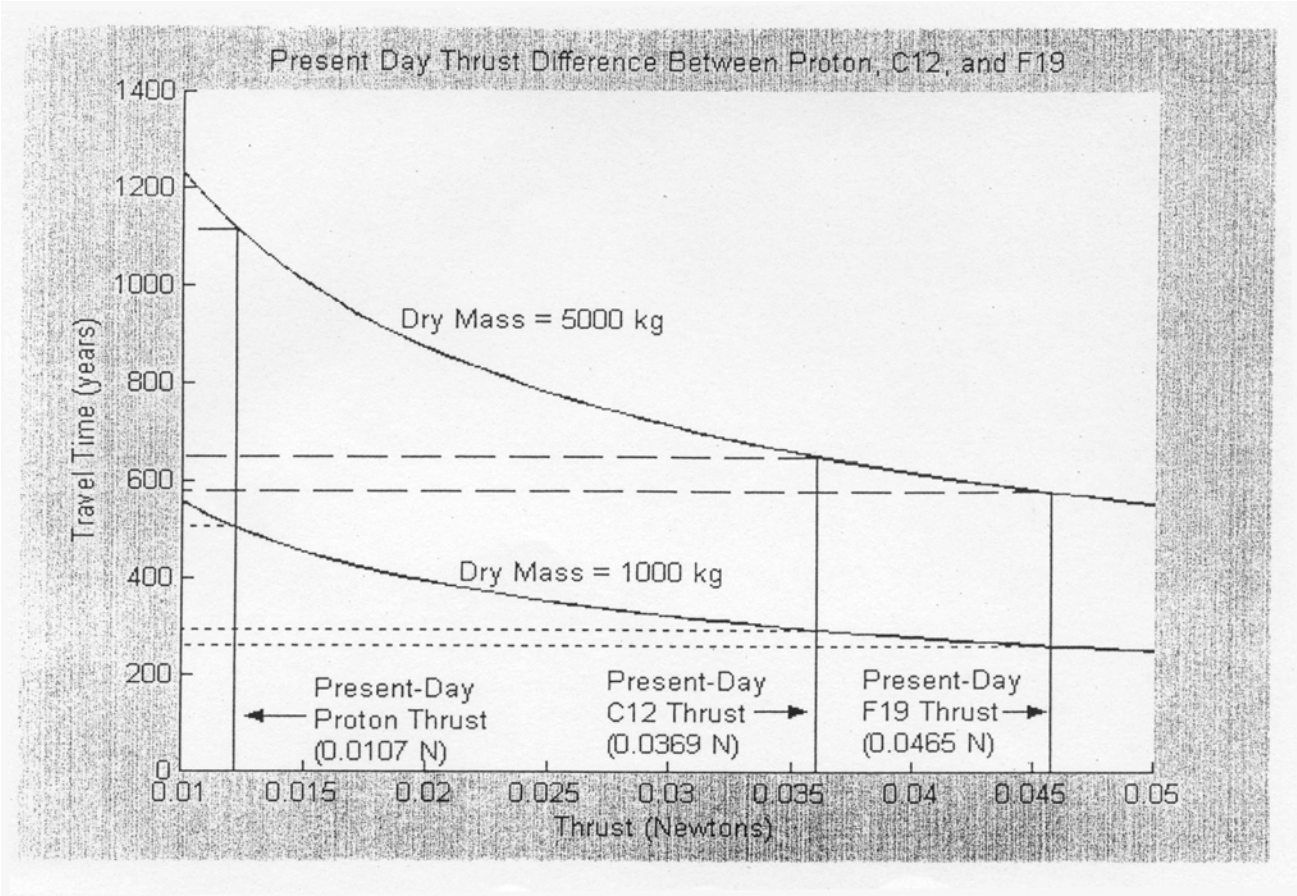

Fig. 10. Oort Cloud mission with heavier ions

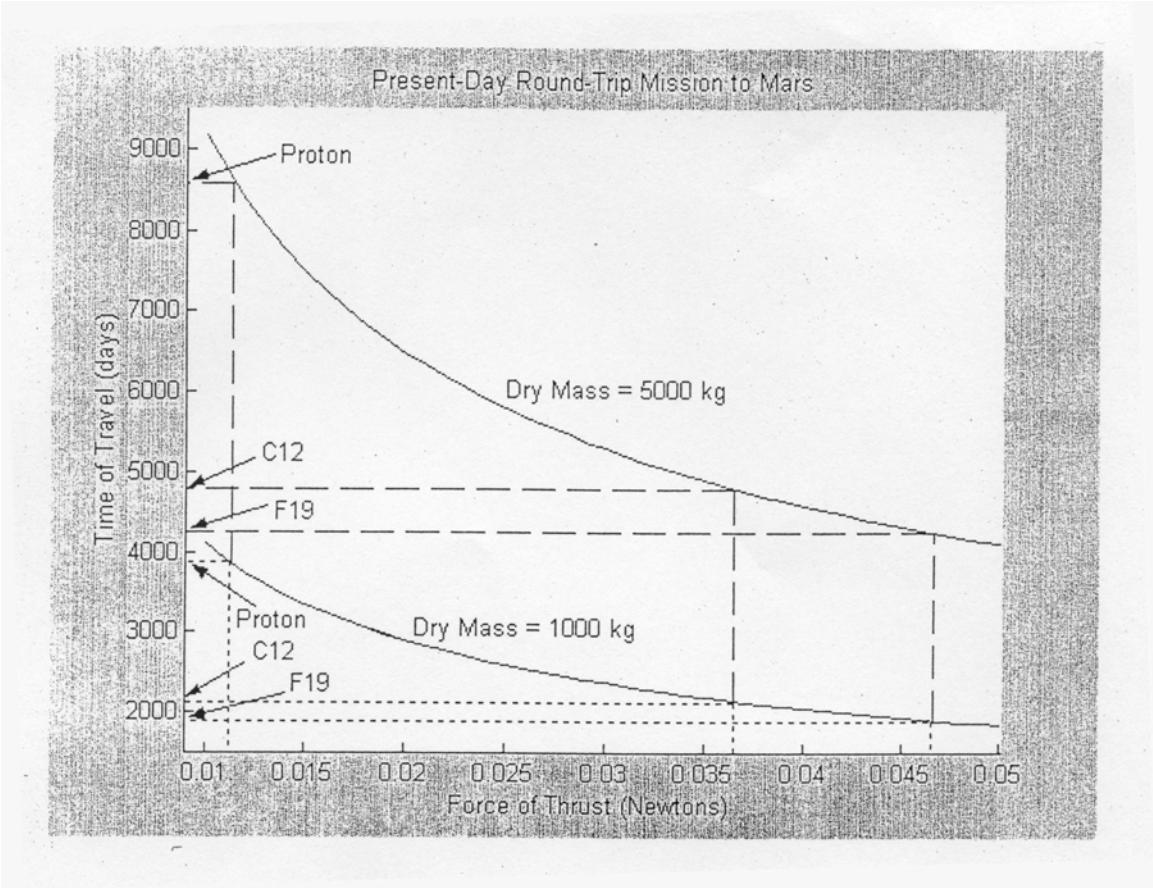

Fig. 11. Mars mission with heavier ions

Table 3

Oort cloud travel time with proton, carbon and fluorine ion thrusters

Vehicle mass	Proton Thrust (N) Time (yr)	Carbon Thrust (N) Time (yr)	Fluorine Thrust (N) time (yr)
5000 kg	0.011 1193	0.037 643	0.047 574
1000 kg	0.011 540	0.037 290	0.047 259

Table 4

Mars Mission with Proton, Carbon and Fluorine in thrusters

Vehicle mass	Proton Thrust (N) Time (d)	Carbon Thrust (N) Time (d)	Fluorine Thrust (N) time (d)
5000 kg	0.011 8875	0.037 4769	0.047 4251
1000 kg	0.011 3969	0.037 2133	0.047 1901

which for large aspect ratio, i.e. L >> t , it reduces to $d = 2t$ indicating that the hydraulic diameter depends only on the thickness of the jet. In order to maintain a laminar flow, the Reynolds number must be less than approximately 1000. This leads to a maximum velocity that is dependent on the jet thickness and the kinematic viscosity of the liquid, hence

$$\mathrm{v} \le \frac{50\,\eta\left[10^{-7}\ \mathrm{m}^2/\mathrm{s}\right]}{\mathrm{t}\,(\mu\mathrm{m})}\,\mathrm{m}/\mathrm{s} \qquad (34)$$

A preliminary analysis using Gallium ($\eta = 3\times10^{-7}\ \mathrm{m}^2/\mathrm{s}$) and a jet thickness of 1000 μm gives a maximum fluid speed of $\mathrm{v} \le 1.5\,\mathrm{m/s}$ before the jet becomes turbulent. When the jet thickness is reduced to 10 μm the maximum speed is increased to $15\,\mathrm{m/s}$. From an energy balance using Bernoulli's equation to obtain a Gallium fluid speed of $10\,\mathrm{m/s}$, a pressure of about 45 psi (3 atm) is required.

The Rayleigh instability, which arises when the Reynolds number exceeds the value noted above, causes the jet beam to spontaneously form

"droplets". While the interaction of the laser with these droplets may be useful for the production of x-ray, the droplet shape will also result in a strong focusing of the proton beam that arises from such an interaction, a desirable effect from the viewpoint of propulsion. The droplet formation occurs through minimization of the surface energy, and for a round jet, it occurs at a distance from the nozzle orifice of

$$L_d = 12\,v\left[\sqrt{\frac{\rho D^3}{\sigma}} + \frac{3D\eta}{\sigma}\right] \qquad (35)$$

where ρ is the fluid density, D the jet diameter, and σ the surface tension of the fluid. For a 15 μm round Gallium jet at $10\,m/s$, the droplet formation length is approximately 1 mm. While quite small, this distance should be sufficient to provide adequate space to focus a 1 μm laser spot. It is expected that the droplet formation length of the non-circular jet will be approximately equivalent to the droplet formation length of a circular beam. A series of experiments using 30 μm round Gallium jets produced x-rays, and those using 10 μm water jets produced protons (See Fig 12). Because of the high Z (charge number) of Gallium, there was a greater number of electrons available to participate in the acceleration of protons (see the electron cloud model) as compared to water. The source of the protons is apparent in the case of the water jet. In the Gallium case the protons originate from a surface layer of water that naturally adheres to Gallium metal. With a Gallium-water combination, the proton source is not limited by the number of electrons available from a water molecule. In summary, these studies have shown that suitable jet targets can indeed be employed in a LAPPS propulsion concept to provide the 1 kHz repetition

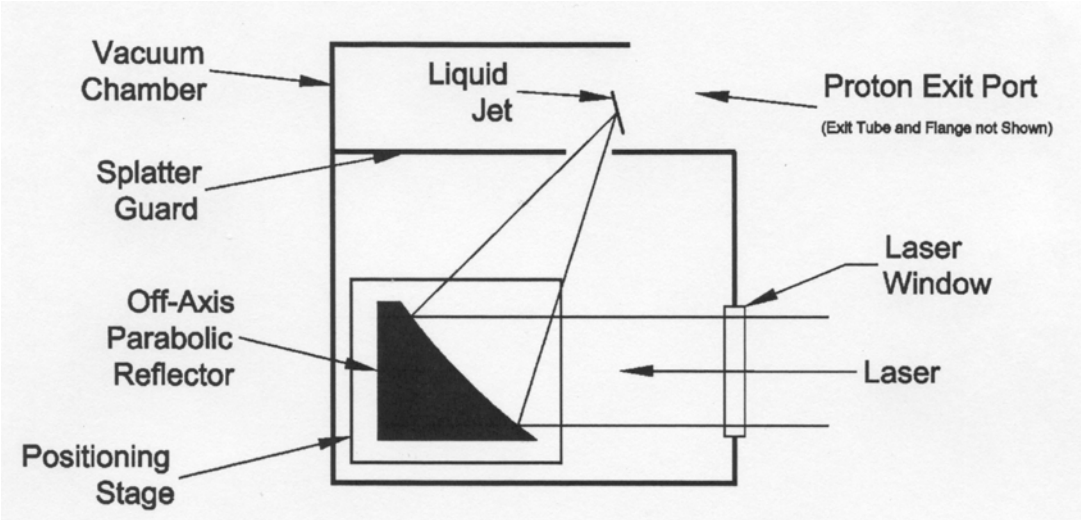

Fig. 12. Schematic layout of interaction chamber

rate needed for generating the propulsion parameters alluded to earlier.

Conclusion

We have presented in this report a propulsion concept that is expected to evolve out of world-wide research in the area of ultrafast laser acceleration of charged particles to relativistic energies. Using recent experimental data in this field, we have introduced the LAPPS propulsion scheme, which we have shown to be capable of producing millions of seconds of specific impulse albeit at modest thrusts. While present-day LAPPS may be viewed as adequate for an interstellar mission such as that to the Oort cloud, it is found to be inadequate for interplanetary missions due to the small thrusts it generates. Several schemes for enhancing the thrust have been proposed including irradiation of larger focal spots, and the acceleration of heavy ion such as those of carbon and fluorine, and more recently lead in place of protons. It was also demonstrated, on the basis of detailed analysis of the ion gas expansion in vacuum, that larger focal spots lead to more efficient energy transfer to these ions from the laser with the additional increase in the velocity contributing directly to thrust enhancement. Moreover, we have demonstrated the feasibility of using jet targets for high rep rates or quasi steady state operations. It is suggested that, with the rapid developments in laser technology particularly as they pertain to ultra high intensity capabilities; unrivaled space propulsion systems will soon emerge.

References

1. Umstadter, D, Journal of Physics D: Applied Physics 36, 151 (2003).
2. Landau and Lifschitz "The Classical Theory of Fields" Addison-Wesley Publishing Company, Inc. Boston (1969).
3. Sarachik and Schappert, G., Phys. Rev. D 1, 2738 (1970).

4. Chen,S., Maksimchuk, A and Umstadter, D., Nature 396, 653 (1998). See also Chen, S et al, Phys. Rev. Letters, 84, 5528 (2000).
5. Yu, W. et al, Phys. Rev. E., 58, 2456 (1999).
6. Tikhonchuk, V.T., Phys. Plasmas 9, 1416 (2002).
7. Maksimchuk, A., Gu, A., Flippo, K and Umstadter, D., Phys. Rev. Letters, 84, 4108 (2000).
8. Gurevich, A.A., et al, Sov. Phys. JETP 22, 449 (1966).
9. Kovalev, V.F., et al, JETP Letters 74, 10 (2001).
10. Dorozkhina, D.S., and Semenov, V.E., Phys. Rev. Letters 81, 2691 (1998).
11. Mora, P., Phys. Rev. Letters, 90, 18500 (2003).
12. Snavely, R.A. et al, Phys. Rev. Letters 85, 2945 (2000).
13. Roth, M., et al, Proc. 1st Int. Conf on Martial Fusion Sciences and Applications, Bordeaux, France, Sept 12-17 (1999). Also UCRL-JC-135735, Sept. 16 (1999)
14. Mason, L., NASA Glenn. Res. Center Private Communication (2001)
15. Kammash, T., J. Propulsion and Power 16, 1100 (2000).
16. Kammash, T., "Fusion Energy in Space Propulsion" AIAA Progress in Astronautics and Aeronautics vol. 167, Washington, D.C. (1995) p.69.
17. Woodcock, G. et al, "Benefits of Nuclear Electric Propulsion for Outer Planet Exploration," 38th Joint Propulsion Conference, Indianapolis, 7-10 July (2002), paper AIAA 2002-3548.
18. Clark, E.L. et al, Phys. Rev. Letters 85, 1654 (2000).
19. Hegelich, M, et al, Phys. Rev. Letters 89, 08500 (2002).
20. Berglund, M. et al, Reviews of Scientific Instruments, 69, 2361 (1998).